A nonlinear analysis of laying a floating pipeline on the seabed

Jaime García-Palacios , Avelino Samartin, Vicente Negro

A B S T R A C T

In this article, a model for the determination of displacements, strains, and stresses of a submarine pipeline during its construction is presented. Typically, polyethylene outfall pipelines are the ones treated by this model. The process is carried out from an initial floating situation to the final laying position on the seabed. The following control variables are considered in the laying process: the axial load in the pipe, the flooded inner length, and the distance of the control barge from the coast. External loads such as self-weight, dead loads, and forces due to currents and small waves are also taken into account.

This paper describes both the conceptual framework for the proposed model and its practical application in a real engineering situation. The authors also consider how the model might be used as a tool to study how sensitive the behavior of the pipeline is to small changes in the values of the control variables. A detailed description of the actions is considered, especially the ones related to the marine environment such as buoyancy, current, and sea waves.

The structural behavior of the pipeline is simulated in the framework of a geometrically nonlinear dynamic analysis. The pipeline is assumed to be a two-dimensional Navier–Bernoulli beam. In the nonlinear analysis an updated Lagrangian formulation is used, and special care is taken regarding the numerical aspects of sea bed contact, follower forces due to external water pressures, and dynamic actions.

The paper concludes by describing the implementation of the proposed techniques, using the ANSYS computer program with a number of subroutines developed by the authors. This implementation permits simulation of the two-dimensional structural pipe behavior of the whole construction process. A sensitivity analysis of the bending moments, axial forces, and stresses for different values of the control variables is carried out. Using the techniques described, the engineer may optimize the construction steps in the pipe laying process.

Keywords:
Pipeline construction
Nonlinear analysis

1. Introduction

Predicting the structural behaviour of a submarine pipeline and controlling it during the laying process is a complex problem. In fact, in this process different aspects should be considered. First, it is necessary to float the long flexible pipe, usually made of high density polyethylene, over its final position. Second, a cable is attached to one end of the pipe and secured to a location on the coast. The other end is attached to a controlling barge. Finally, the pipe is flooded with water. The additional mass of water should cause the outfall pipe to sink to its final position on the sea floor. The control parameters considered in the laying process include an imposed axial force on the structure, the distance of the boat from the coast, and the velocity at which the pipe is filled with water from the end close to the coast.

Typically, in order to start the described laying process a number of other activities are carried out beforehand. Some of these activities include:

- The manufacture of the pipes.
- Where a long outfall pipeline is required, the pipes need to be joined together. A long outfall pipe is usually floated relatively close to its final position, inside a harbor or estuary, thus protecting it from rough seas.
- A trench may be excavated by dredging in the location where the outfall pipeline is to be placed.
- The structure is towed by tugboats to the construction area.
- The end closest to the coast is connected to a previously existing pipeline or to the coast itself by means of a cable.
- The outfall pipeline is placed, at a previously decided position, over the stinger located in the control barge. An axial load is applied at the same position.
- The outfall pipeline is flooded from the end close to the coast at a given velocity. At the same time the barge advances whilst passing out more pipeline and adjusting the axial load.

During this process, the outfall pipeline will adopt an S-shaped geometry which is governed by the different possible combinations of the control variables over time, that is, the inundated length, the position of the barge, and the applied axial load.

The structural model described in this paper can be used as an analytical tool in order to optimize the stresses appearing during the laying process, i.e. as a solution to a problem of optimal control [3].

2. An overview of structural models for the analysis of pipelines

Over the past few decades, there has been intensive development of models for the process described. This development was mainly caused by the increasing power of computation and by the investment made by oil companies to reduce contamination risk during the loading and unloading of oil tankers in buoys connected by means of flexible pipelines. In general, while oil pipelines are more flexible and placed deeper on the sea bed than outfall pipelines, advances in the first field can be applied to the second one.

Pipeline stress analysis requires knowledge of disciplines such as marine hydrodynamics and solid mechanics. Hydrodynamics is necessary to define the actions according to the wave theory adopted in each case and to study the interaction between the fluid and structure. Solid mechanics is needed to develop the suitable geometrically nonlinear analysis of the pipeline structural behavior due to external actions. From this analysis the optimal response of the pipeline can be reached.

Several types of outfall pipeline structural analyses can be applied. These differ according to the following characteristics:

- Existence of inertial forces (static and dynamic nonlinear analysis).
- Representation of the pipeline (beam and shell structure).
- Number of degrees of freedom per node (3 and 6 for two-dimensional and three-dimensional analysis, respectively). In the case of a three-dimensional analysis, it is possible to study the pipeline behavior subjected to forces that are acting out of the plane in which it is placed, those produced by transversal current and skew waves, for example.

Outfall analysis has been the subject of several standards and recommendations. State-of-the-art descriptions based on experiences in the energy sector can be cited. These include the practical oriented [4] or the more theoretical [5]. Despite the significant advances reached in the area, further work is needed. In a recent review, [6] describes more up-to-date techniques for pipeline analysis which include dynamic models, that take into account both the time domain and frequency domain. The paper highlights the need for a improved simulation techniques for the hydrodynamic actions, with the associated damping coefficients and the interaction between the fluid and the structure. This need is particularly relevant in the area of contact between the sea bed and the structure. This knowledge improvement could be achieved according to [6] through extensive and specialized experimentation.

The first pipeline analyses were carried out assuming a catenary behavior for the pipe, i.e. as a cable. The cable geometry is successively modified in order to include bending stiffness. In [7], the bending stiffness is reached by incremental load steps. In [8], hybrid methods, a combination of load increments and iterative analysis, are used. As time progressed, the methods evolved, introducing some rigidity to the cable, thus approximating the influence of the bending stiffness of the pipeline. The differential equation derived from this kind of model is solved in [9] by means of finite difference techniques. According to the initial and boundary conditions, sea bottom contact can be simulated. A more sophisticated numerical analysis of this problem is described in [10]. Some semi-analytical solutions including nonlinear beam–column and elastic Winkler soil finite elements are shown in [11].

At the present time, most of the specific computer programs used to solve this type of problem are based on finite elements. However, general commercial finite element software programs such as SAP [12], ABAQUS [13], or ANSYS [14] are not very suitable for simulating the laying of a floating outfall pipeline on the seabed. They are capable of solving parts of the process such as large displacement, plasticity, and contact problems, i.e. they can typically be applied assuming a fixed position of the pipe. However, if the software is used to model the whole process, then numerical difficulties arise when trying to simulate the movement of the barge, the changing length of flooded pipeline, and the applied axial load. Furthermore, most of the loads considered in this problem are *follower forces*, as described in [15]. These forces, due to waves, current, and water pressure, are dependent on the deformed geometry of the structure, and these follower forces should be accurately simulated within each load step. In contrast, if follower forces are treated as standard forces small errors at each computational step can be accumulated, leading to unsatisfactory results after several iterations.

In [16], different theoretical scenarios are described that could be used to handle the nonlinear analysis of pipeline laying. These include the total Lagrangian, updated Lagrangian, and even Eulerian formulations. Typically, the last formulation is often used in hydrodynamics. From a different point of view, [17] concentrates on the computational details that need to be carried out at each step. However, the mathematical framework is not discussed in detail.

In the oil industry some works have taken into account other aspects of the analysis. These can be considered of secondary importance for outfall pipelines. These aspects are listed as follows:

- Cross-sectional ovalization and buckling is discussed in [18–21] and [22].
- The influence of the internal high speed flow and the axial stress on the pipe is studied in [23].
- The flow field changes and vortex shedding due to the existence of a pipeline with a given diameter, and also when this outfall is close to a boundary layer such as the sea bed, is dealt with by [11].

The report published by CIRIA [24], which includes a specific chapter dedicated to the design of this type of pipeline, should also be mentioned.

In the professional domain, there exist a number of specific computer programs that have been developed to analyze the structural behavior of the pipeline laying problem. An interesting example is *NV457 Static and Dynamic Analysis of Marine Pipeline during laying* developed in Norway by Det Norske Veritas. In Spain the initial work of [1] and most recently [25,2] are examples of this development, as well as some in-house programs used by specialist enterprises such as [26].

3. Model description

3.1. Hypotheses

In this section we present a model which is used to simulate the behavior of the outfall pipeline during the construction process. The model is specifically used to study the evolution of the geometry, deformed shape, and stresses right up to the time when the pipeline has been laid on the sea bed.

3.1.1. Hypotheses of pipe laying

The hypotheses considered in the model are summarized as follows:

1. The pipeline is passed out into the sea through a stinger situated at mean sea level (MSL). This stinger can be modeled either as a straight ramp with constant slope or as a constant curvature ramp.
2. The process is irreversible. For example, when a part of the outfall pipeline has reached the sea bed, it cannot be lifted again.
3. The sea bed is considered to be a continuous line that can have different slopes. It is located in the same vertical plane as the pipeline.

With hypothesis 1 the pipe behavior in the barge is intended to be simulated. In this respect, the following simplifications have been introduced:

- There is no movement out of the plane of the pipeline.
- The dynamic effects of the contact between the pipe and the stinger are neglected.
- The dynamic movements of the barge are not considered, even the ones due to the axial deformation of the outfall.
- The coefficient of slip between the pipe and the stinger is zero.

The first three simplifications are acceptable when a large barge and small waves are considered, circumstances that are quite common.

3.1.2. Hydrodynamic hypotheses

1. The fluid is considered to be incompressible.
2. The Airy Linear Wave Theory is applied to study the sea movements.
3. The sea state is represented by a constant period T and the wave number $k = \frac{2\pi}{L}$, with $L = f(h)$ the wavelength given as a function of the sea depth.
4. The velocity and acceleration fields due to waves are not modified by the existence of the pipeline.
5. The characteristics of the velocity and acceleration fields are obtained for a given number of discrete subdivisions of the continuous sea bed. Depth is calculated as the mean depth of the subdivision under consideration.
6. The transformation of the sea waves from sea to coast is supposed to occur within the plane of the outfall.

3.1.3. Structural hypotheses

1. The behavior of the pipeline is modeled as a two-dimensional beam with a circular cross-section subject to axial and bending deformations. This model is developed in the framework of the finite element method. The total length of the outfall (L_T) is divided into N two-node elements with equal length and three degrees of freedom per node (two displacements and one rotation).
2. The pipe material is linear elastic.
3. Torsional and shear deformation are not considered.
4. Rotational inertia forces are neglected.

3.2. Actions

The pipeline is subjected to the following actions:

- Constant direction actions:
  - Self-weight. This action is found assuming each pipe element out of the water, for both empty and flooded conditions.
  - An axial load is applied from the barge.
  - A barge displacement, that has the pipe longitudinal direction, i.e. the global X direction.
  - Contact reactions between the sea bed and the pipeline.

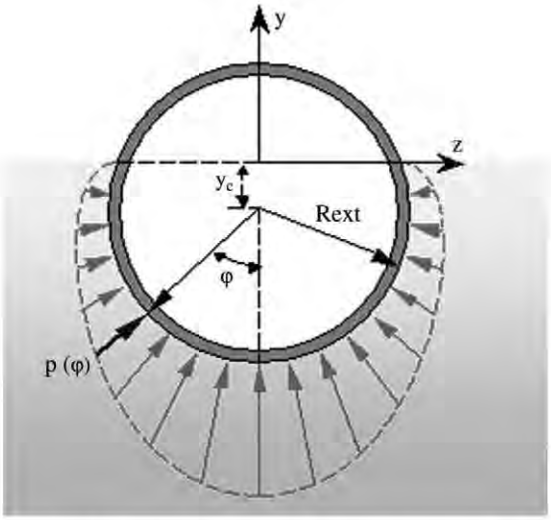

Fig. 1. Hydrostatic cross-section pressure distribution.

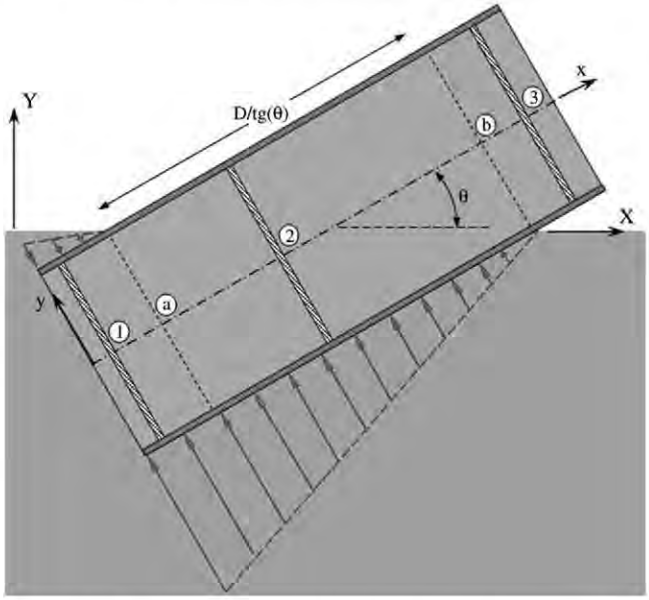

Fig. 2. Hydrostatic pressure distribution along the pipeline.

- Follower loads.

  The forces are due to the following two sources:

  1. Hydrostatic pressure.

     In most models this action is considered as a self-weight reduction, i.e. as a difference between the submerged and the air weight of the pipe element. This common simplification has not been applied to the present model.

  2. Sea waves and current loads.

     These loads are computed through the Morison et al. [27] transformation of the velocity and acceleration fields.

These two actions along the outfall pipeline are described as follows.

1. Hydrostatic pressure.

The distribution of hydrostatic pressure along the cross-section of the pipeline is shown in Fig. 1. The longitudinal variation of the resultant can be seen in Fig. 2, where three different situations are computed.

The hydrostatic pressure at a section normal to pipe axis is given by the following expressions:

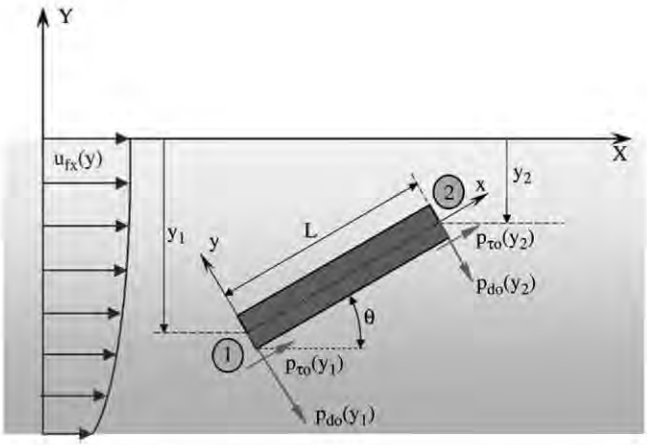

Fig. 3. Current velocity distribution and force components along the element.

(a) Pipeline out of water: $y_c \geq R_{ext}\cos\theta$

$$p(\varphi) = 0 \tag{1}$$

$$p_h(y_c) = 0. \tag{2}$$

(b) Semi-submerged pipeline: $R_{ext}\cos\theta \geq y_{cL} \geq -R_{ext}\cos\theta$

$$p(\varphi) = \gamma_w\,[R_{ext}\cos\varphi\cos\theta - y_c] \quad \text{with: } \varphi_c \geq \varphi \geq -\varphi_c \tag{3}$$

$$p_h(y_c) = \gamma_w R_{ext}^2\cos^2\theta\left[\arccos\left(\frac{y_c}{R_{ext}\cos\theta}\right) - \frac{y_c}{R_{ext}\cos\theta}\sqrt{1-\left(\frac{y_c}{R_{ext}\cos\theta}\right)^2}\right] \tag{4}$$

where $\varphi_c = \arccos\left(\frac{y_c}{R_{ext}\cos\varphi}\right)$.

(c) Submerged pipeline: $y_{cL} \leq -R_{ext}\cos\theta$

$$p(\varphi) = \gamma_w\,[R_{ext}\cos\varphi\cos\theta - y_c] \quad \text{con: } -\pi \geq \varphi \geq \pi \tag{5}$$

$$p_h(y_c) = \gamma_w \pi R_{ext}^2\cos^2\theta \tag{6}$$

with y_c the global Y coordinate of the pipeline cross-section centre, $p(\varphi)$ the hydrostatic pressure intensity, and γ_w the specific weight of water. The resultant vertical uplift force is designed by p_h.

In addition to these hydrostatic pressure forces along the pipeline the force and moment resultants of these forces at the end pipeline section have been evaluated.

2. Stationary horizontal current.

This action produces a depth varying velocity distribution, $u_{fc}(y)$, as shown in Fig. 3.

This current generates a drag force (p_{d_0}) over a vertical cylinder ($\theta = \pi/2$) given by

$$p_{d_0} = \frac{1}{2}C_d\rho_w D|u_{fc}|u_{fc} \tag{7}$$

according to Morison et al. [27], with C_d the drag coefficient.

When the pipeline element is inclined at angle θ, the drag force has normal and tangential components. Their corresponding values are obtained as follows:

- Normal follower load due to the normal velocity:

The velocity of the current normal to the pipeline is

$$u_{f_v} = u_{fc}\sin\theta \quad \text{with } -\frac{\pi}{2} \leq \theta \leq \frac{\pi}{2} \tag{8}$$

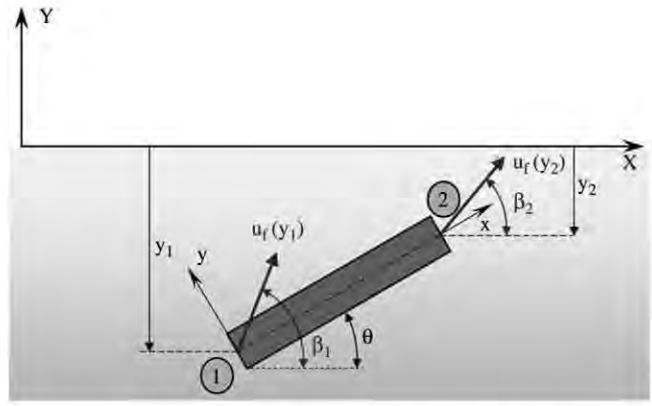

Fig. 4. Fluid velocities due to a sea wave along the pipeline.

which produces a normal pressure p_d given by

$$p_d(y) = \frac{1}{2}C_d\rho_w D|u_{fc}(y)\sin\theta|u_{fc}(y)\sin\theta = \varepsilon_1\frac{1}{2}C_d\rho_w D u_{fc}^2(y)\sin^2\theta = \varepsilon_1 p_{d_0}(y)\sin^2\theta \tag{9}$$

where

$$p_{d_0}(y) = \frac{1}{2}C_d\rho_w D u_{fc}^2(y) \tag{10}$$

and $\varepsilon_1 = 1$ if $u_{fc}\sin\theta \geq 0$ and $\varepsilon_1 = -1$ if $u_{fc}\sin\theta \leq 0$.

- Tangential follower load, obtained from the general expression of Morison et al. [27] equation:

$$p_\tau = C_t\rho_w\frac{D}{2}|\mathbf{u}_f|u_{f_\tau} \tag{11}$$

where $\mathbf{u}_f = u_{f_x}\mathbf{x}$ and $u_{f_\tau} = \mathbf{u}_f\boldsymbol{\tau}$, with $\mathbf{x}$ and $\boldsymbol{\tau}$ the unit vectors in the X and tangential directions, respectively. In this case, $u_{fx} = u_{fc}$ and $u_{f_\tau} = u_{fc}\cos\theta$.

Therefore,

$$p_\tau = p_\tau(y) = C_t\rho_w\frac{D}{2}u_{fc}(y)\cos\theta = p_{\tau_0}(y)\cos\theta \tag{12}$$

with $p_{\tau_0}(y) = C_t\rho_w\frac{D}{2}u_{fx}(y)$.

3. Two-dimensional waves.

This action introduces velocity ($\mathbf{u}_f$) and acceleration ($\dot{\mathbf{u}}_f$) fields that are dependent on the time and spatial coordinates, as shown in Fig. 4.

The application of the generalized Morison et al. [27] equation leads to the normal pressure:

$$p_v = C_I A_I\dot{u}_{f_v} + C_D A_D|u_{f_v}|u_{f_v} \tag{13}$$

with

$$\mathbf{u}_f(x,y,t) = u_{f_\tau}\boldsymbol{\tau} + u_{f_v}\boldsymbol{v} = u_f\mathbf{x} + v_f\mathbf{y} = u_{f_0}\,[\cos\beta\,\mathbf{x} + \sin\beta\,\mathbf{y}] \tag{14}$$

$$\dot{\mathbf{u}}_f(x,y,t) = \dot{u}_{f_\tau}\boldsymbol{\tau} + \dot{u}_{f_v}\boldsymbol{v} = \dot{u}_f\mathbf{x} + \dot{v}_f\mathbf{y} = \dot{u}_{f_0}\,[\cos\beta\,\mathbf{x} + \sin\beta\,\mathbf{y}] \tag{15}$$

where ($\boldsymbol{v}$) and ($\boldsymbol{\tau}$) are the normal and tangential unit vectors respectively (in relation to the pipeline) and $\mathbf{x}$ and $\mathbf{y}$ are the Cartesian unit vectors. The relationships between the different components of velocity and acceleration are

$$u_{f_0} = \left(u_f^2 + v_f^2\right)^{\frac{1}{2}}, \quad \tan\beta = \frac{v_f}{u_f} \tag{16}$$

$$\dot{u}_{f_0} = \left(\dot{u}_f^2 + \dot{v}_f^2\right)^{\frac{1}{2}}, \quad \tan\beta = \frac{\dot{v}_f}{\dot{v}_f}. \tag{17}$$

The velocity field is defined in general Cartesian axes as

$$\mathbf{u}_f = u_f(\cos\beta\mathbf{x} + \sin\beta\mathbf{y}) = u_f^0\mathbf{x} + v_f^0\mathbf{y} \tag{18}$$

where $u_f = u_f(x, y, t)$ and $\beta = \beta(x, y, t)$.

Vector $\mathbf{u}_f$ has an angle $\beta - \theta$ with the element direction, and can be written as

$$\mathbf{u}_f = u_f[\cos(\beta-\theta)\boldsymbol{\tau} + \sin(\beta-\theta)\boldsymbol{\nu}]. \tag{19}$$

The acceleration field can be derived in a similar way:

$$\begin{aligned}\dot{u}_f &= \dot{u}_f\left[\cos(\overline{\beta}-\theta)\boldsymbol{\tau} + \sin(\overline{\beta}-\theta)\boldsymbol{\nu}\right]\\ &= \frac{2\pi}{T}u_f\left[\sin(\overline{\beta}-\theta)\boldsymbol{\tau} - \cos(\overline{\beta}-\theta)\boldsymbol{\nu}\right]\end{aligned} \tag{20}$$

where $\overline{\beta} = \beta + \frac{\pi}{2}$.

According to the Airy Linear Wave Theory the following expression can be obtained:

$$u_{f0} = \frac{H}{2}\frac{gT}{L}\frac{1}{\cosh\frac{2\pi d}{L}}(C_f^2c_f^2 + S_f^2s_f^2)^{\frac{1}{2}};$$

$$\dot{u}_{f0} = \frac{g\pi H}{L}\frac{1}{\cosh\frac{2\pi d}{L}}(C_f^2s_f^2 + S_f^2c_f^2)^{\frac{1}{2}} \tag{21}$$

where

$$C_f = \cosh\frac{2\pi}{L}(y+d) \quad S_f = \sinh\frac{2\pi}{L}(y+d) \tag{22}$$

$$c_f = \cos\theta_f \quad s_f = \sin\theta_f \quad \theta_f = \frac{2\pi}{L}x - \frac{2\pi}{T}t \tag{23}$$

$$\dot{u}_{f0} = \frac{g\pi H}{L}\frac{1}{\cosh\frac{2\pi d}{L}}(C_f^2s_f^2 + S_f^2c_f^2)^{\frac{1}{2}} \tag{24}$$

$$\tan\beta = \tanh\frac{2\pi}{L}(y+d)\tan\theta_f \tag{25}$$

$$\tan\overline{\theta} = -\tanh\frac{2\pi}{L}(y+d)\cot\theta_f \tag{26}$$

with L the wavelength, T the period, and d the sea depth.

The normal follower load is

$$f_v = C_IA_I\dot{u}_{f0}\sin(\overline{\beta}-\theta) + C_DA_D\left|u_{f0}\sin(\beta-\theta)\right|\sin(\beta-\theta)u_{f0}. \tag{27}$$

The element force resultants at the end nodes α ($\alpha = 1, 2$) are

$$p_{v_1} = \frac{L}{6}\left[2f_{v_1} + f_{v_2}\right] \qquad p_{v_2} = \frac{L}{6}\left[f_{v_1} + 2f_{v_2}\right] \tag{28}$$

with

$$\begin{aligned}f_{v_\alpha} &= f_v(x_\alpha, y_\alpha, t) = C_IA_I\dot{u}_{f0}\sin(\overline{\beta}_\alpha - \theta)\\ &\quad + C_DA_D\left|u_{f0\alpha}\sin(\beta_\alpha-\theta)\right|\sin(\beta_\alpha-\theta)u_{f0\alpha}\end{aligned} \tag{29}$$

and

$$\dot{u}_{f0\alpha} = \dot{u}_{f0}(x_\alpha, y_\alpha, t) \tag{30}$$

$$u_{f0\alpha} = u_{f0}(x_\alpha, y_\alpha, t) \tag{31}$$

$$\overline{\beta}_\alpha = \overline{\beta}(x_\alpha, y_\alpha, t) \tag{32}$$

$$\beta_\alpha = \beta(x_\alpha, y_\alpha, t) \quad (\alpha = 1, 2). \tag{33}$$

It is convenient to separate these forces into two components: the inertia forces f_v^I due to the acceleration and the drag forces f_v^D due to the velocity. The latter component can be treated similarly to that of the previous case 2, that is, as a stationary horizontal current. Then

$$f_v = f_v^I + f_v^D \tag{34}$$

with

$$f_v^I = C_IA_I\dot{u}_{f0}\sin(\overline{\beta}-\theta) = k^I\sin(\overline{\beta}-\theta)\dot{u}_{f0} \tag{35}$$

$$\begin{aligned}f_v^D &= C_DA_D\left|u_{f0}\sin(\beta-\theta)\right|u_{f0}\sin(\beta-\theta)\\ &= k^D\varepsilon_1u_{f0}^2\sin^2(\beta-\theta)\end{aligned} \tag{36}$$

and

$$\varepsilon_1 = 1 \quad \text{si} \quad u_{f0}\sin(\beta-\theta) > 0 \tag{37}$$

$$\varepsilon_1 = -1 \quad \text{si} \quad u_{f0}\sin(\beta-\theta) < 0. \tag{38}$$

3.3. Matrices and vectors of the pipe element

An updated Lagrangian formulation (UL) is used to determine the movements and stresses of the pipeline.

The stiffness matrix for a general three-dimensional beam element can be obtained from the incremental Principle of Virtual Work, between configurations C_1 and C_2. In the following, standard notation, as presented in [28], and the repeated index sum convention will be used. Applying a UL formulation to a solid in equilibrium in the C_1 configuration, the following expression is reached:

$$\int_{{}_1V}{}_1S_{ij}\,{}_1\varepsilon_{ij}^{*\,1}\mathrm{d}V + \int_{{}_1V}{}^1\sigma_{ij}\,{}_1\eta_i^{*\,1}\mathrm{d}V = {}_1^2R - {}_1^1R$$

$$(i, j = 1, 2, 3) \tag{39}$$

where

$${}_1^1R = \int_{{}_1V}{}^1\sigma_{ij}\,{}_1e_{ij}^{*\,1}\mathrm{d}V = \int_{{}_1S}{}_1^1t_iu_i^{*\,1}\mathrm{d}S + \int_{{}_1V}{}_1^1f_iu_i^{*\,1}\mathrm{d}V \tag{40}$$

$${}_1^2R = \int_{{}_1S}{}_1^2t_iu_i^{*\,1}\mathrm{d}S + \int_{{}_1V}{}_1^2f_iu_i^{*\,1}\mathrm{d}V \tag{41}$$

is the virtual work due to the external forces measured from the C_1 configuration.

The virtual Green strain can be expressed as a sum of linear and nonlinear components:

$${}_1\varepsilon_{ij}^* = {}_1e_{ij}^* + {}_1\eta_{ij}^* \tag{42}$$

where

$${}_1e_{ij}^* = \frac{1}{2}\left(\frac{\partial u_i^*}{\partial\,{}^1x_j} + \frac{\partial u_j^*}{\partial\,{}^1x_i}\right) \tag{43}$$

$${}_1\eta_{ij}^* = \frac{1}{2}\left(\frac{\partial u_k^*}{\partial\,{}^1x_i}\frac{\partial u_k}{\partial\,{}^1x_j} + \frac{\partial u_k}{\partial\,{}^1x_i}\frac{\partial u_k^*}{\partial\,{}^1x_j}\right). \tag{44}$$

Eq. (39) expresses the change in virtual work due to the increment of the external forces ${}_1^2R - {}_1^1R$ to go from C_1 to C_2.

Eq. (39) can be modified by introducing terms of incremental updated Green strains, instead of incremental updated Kirchhoff stresses. This transformation can be achieved by using the material constitutive equations ${}^1\sigma_{ij} = C_{ijkl}\,{}_1\varepsilon_{kl}$, and then the following equation is obtained:

$$\int_{{}_1V}{}_1C_{ijkl}\,{}_1\varepsilon_{kl}\,{}_1\varepsilon_{ij}^{*\,1}\mathrm{d}V + \int_{{}_1V}{}^1\sigma_{ij}\,{}_1\eta_{ij}^{*\,1}\mathrm{d}V = {}_1^2R - {}_1^1R. \tag{45}$$

Eqs. (39) and (45) cannot be directly solved in terms of the displacement variables, because they are nonlinear functions of the displacement increments.

Approximate exact solutions can be obtained using the following two approximations:

$${}_1S_{ij} \approx {}_1C_{ijkl}\,{}_1e_{kl} \tag{46}$$

$${}_1\varepsilon_{ij}^* \approx {}_1e_{ij}^*. \tag{47}$$

Therefore, Eq. (45) can be linearized as

$$\int_{{}_1V}{}_1C_{ijkl}\,{}_1e_{kl}\,{}_1e_{ij}^{*\,1}\mathrm{d}V + \int_{{}_1V}{}^1\sigma_{ij}\,{}_1\eta_{ij}^{*\,1}\mathrm{d}V = {}_1^2R - {}_1^1R. \tag{48}$$

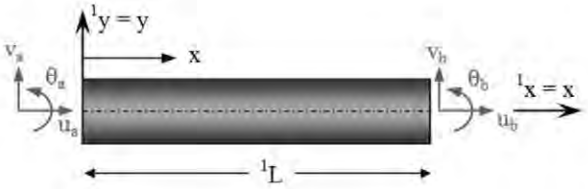

Fig. 5. A two-dimensional beam element in the C_1 configuration.

3.3.1. Stiffness matrix

Eq. (48) can be applied to a two-dimensional beam in which the Navier–Bernoulli beam hypothesis is introduced. Also conventional two-dimensional beam notation is used (see Fig. 5) and only the nonzero beam stresses and strains are taking into account. In the following it is assumed that only external nodal forces, i.e. at end sections of the beam element, are applied. These forces are denoted by ${}^{k}\mathbf{f}$, $(k = 1, 2)$ and the corresponding nodal displacements by $\mathbf{u}^*$. Their expressions are

$$ {}^{k}\mathbf{f} = \left[{}^{k}F_{xa},\ {}^{k}F_{ya},\ {}^{k}F_{za},\ {}^{k}F_{xb},\ {}^{k}F_{yb},\ {}^{k}M_{zb}\right]^{\mathrm{T}} \quad (k = 1, 2) \tag{49} $$

$$ \mathbf{u}^{\mathrm{T}} = [u_a,\ v_a,\ \theta_a,\ u_b,\ v_b,\ \theta_b]\,. \tag{50} $$

Then, Eq. (48) for the two-dimensional Navier–Bernoulli beam element can be written as follows:

$$ \int_0^{{}^{1}L} \left(EAu'u^{*\prime} + EI_z v'' v^{*\prime\prime}\right) \mathrm{d}x + \frac{1}{2}\int_0^{{}^{1}L} {}^{1}F_x v^{*\prime 2}\mathrm{d}x - \int_0^{{}^{1}L} {}^{1}F_y u^{*\prime} v^{*\prime}\mathrm{d}x = \mathbf{u}^{*T}\left[{}^{2}\mathbf{f} - {}^{1}\mathbf{f}\right] \tag{51} $$

with $u(x)$ and $v(x)$, as well as $u^*(x)$ and $v^*(x)$, the real and virtual displacements at point $(x, 0)$, i.e. the centroid of the cross-section x of the element. The following notation has been used: $(') = \frac{\mathrm{d}}{\mathrm{d}x}$; and the constants EA and EI_z represent the axial and bending stiffness of the beam cross-section. The axial and shear stress resultants at section x are given by $F_x = F_x(x)$ and $F_y = F_y(x)$, respectively, and $M_z = M_z(x)$ is the moment stress resultant at section x. The expressions for these stress resultants are

$$ \begin{aligned} &{}^{k}F_x(x) = {}^{k}F_{xa} = -{}^{k}F_{xb}; \qquad {}^{k}F_y(x) = {}^{k}F_{ya} = -{}^{k}F_{yb} \\ &{}^{k}M_z(x) = {}^{k}M_{zb} + {}^{k}F_{yb}(L - x) = -{}^{k}M_{za} + {}^{k}F_{yb}x. \end{aligned} \tag{52} $$

Eq. (51) is also known as the variational equation of the simplified linearized two-dimensional beam theory [28].

The incremental virtual work due to the external forces applied at the element end nodes, a and b, is given by the expression

$$ {}^{2}_{1}R = \mathbf{u}^{*T}({}^{2}\mathbf{f} - {}^{1}\mathbf{f}) \tag{53} $$

where ${}^{k}\mathbf{f}$, $(k = 1, 2)$ are the external forces applied at end sections of the beam element and the $\mathbf{u}^*$ are the corresponding displacements at the end sections:

$$ {}^{k}\mathbf{f} = \left[{}^{k}F_{xa},\ {}^{k}F_{ya},\ {}^{k}F_{za},\ {}^{k}F_{xb},\ {}^{k}F_{yb},\ {}^{k}M_{zb}\right]^{\mathrm{T}} \quad (k = 1, 2) \tag{54} $$

$$ \mathbf{u}^{\mathrm{T}} = [u_a,\ v_a,\ \theta_a,\ u_b,\ v_b,\ \theta_b]\,. \tag{55} $$

Using the finite element technique, the actual and virtual displacements can be written as

$$ \begin{aligned} u &= \mathbf{N}^1\overline{\mathbf{u}}, \qquad u^* = \mathbf{N}^1\overline{\mathbf{u}}^* \\ v &= \mathbf{N}^3\overline{\mathbf{v}}, \qquad v^* = \mathbf{N}^3\overline{\mathbf{v}}^* \\ \theta &= \mathbf{N}^{3'}\overline{\boldsymbol{\theta}}, \qquad \theta^* = \mathbf{N}^{3'}\overline{\boldsymbol{\theta}}^* \end{aligned} \tag{56} $$

where $\mathbf{N}_1$ and $\mathbf{N}^3$ are respectively the linear interpolation functions and the cubic Hermite functions. The following notation is used: $\mathbf{N}^{3'} = \frac{\mathbf{N}_3}{\mathrm{d}\xi}$, and $\xi = \frac{x}{L}$.

Substituting (56) into (51), and taking into account the beam equilibrium equations between bending moments and shear forces and the fact that $\overline{\mathbf{u}}^*$, $\overline{\mathbf{v}}^*$ and $\overline{\boldsymbol{\theta}}^*$ are arbitrary, the following system of equations is obtained:

$$ \left(\frac{EA}{L} + \frac{{}^{1}F_{xb}}{L}\right)\mathbf{k}_{11}^{110}\overline{\mathbf{u}} + \left[-\frac{{}^{1}M_{za}}{L^2}\left(\mathbf{k}_{13}^{120} - \mathbf{k}_{13}^{121}\right) + \frac{{}^{1}M_{zb}}{L^2}\mathbf{k}_{13}^{121} + \frac{{}^{1}M_{za} + {}^{1}M_{zb}}{L^2}\mathbf{k}_{13}^{110}\right]\overline{\mathbf{v}} = {}^{2}\mathbf{f}_{\mathbf{x}} - {}^{1}\mathbf{f}_{\mathbf{x}} \tag{57} $$

$$ \left(\frac{EI_z}{L^3}\mathbf{k}_{33}^{220} + \frac{{}^{1}F_{xb}}{L}\mathbf{k}_{33}^{110} + {}^{1}F_{xb}\frac{I_z}{AL^3}\mathbf{k}_{33}^{220}\right)\overline{\mathbf{v}} + \left[-\frac{{}^{1}M_{za}}{L^2}\left(\mathbf{k}_{31}^{210} - \mathbf{k}_{31}^{211}\right) + \frac{{}^{1}M_{zb}}{L^2}\mathbf{k}_{31}^{211} + \frac{{}^{1}M_{za} + {}^{1}M_{zb}}{L^2}\mathbf{k}_{31}^{110}\right]\overline{\mathbf{u}} = {}^{2}\mathbf{f}_{\mathbf{y}} - {}^{1}\mathbf{f}_{\mathbf{y}} \tag{58} $$

where

$$ {}^{k}\mathbf{f}_{\mathbf{x}}{}^{\mathrm{T}} = \left[{}^{k}F_{xa},\quad 0,\quad 0,\quad {}^{k}F_{xa},\quad 0,\quad 0\right] \tag{59} $$

$$ {}^{k}\mathbf{f}_{\mathbf{y}}{}^{\mathrm{T}} = \left[0,\quad {}^{k}F_{ya},\quad \frac{{}^{k}M_{za}}{L},\quad 0,\quad {}^{k}F_{yb},\quad \frac{{}^{k}M_{zb}}{L}\right] \tag{60} $$

with $k = 1, 2$ and $\mathbf{k}_{\mathbf{mn}}^{\alpha\beta\gamma} = \int_0^1 \mathbf{N}_{\mathbf{m}}^{\alpha\,\mathrm{T}}\mathbf{N}_{\mathbf{n}}^{\beta}\xi^{\gamma}\mathrm{d}\xi$. The superindices α and β are the α and β order derivatives of the shape function N_m and N_n matrices, and γ is the exponent of the natural coordinate ξ.

This equation can be expressed in a compact way as

$$ \left[{}^{1}\mathbf{k} + {}^{1}\mathbf{k}_{\mathbf{g}}\right]\overline{\mathbf{u}} = {}^{2}\mathbf{f} - {}^{1}\mathbf{f} \tag{61} $$

with $\mathbf{k}$ and $\mathbf{k}_{\mathbf{g}}$ being the linear stiffness matrix and geometric stiffness matrix of the two-dimensional beam, respectively.

3.3.2. Equivalent load vector at element end nodes

A distributed load ${}^{2}_{1}\mathbf{g} = ({}^{2}_{1}g_x(x), {}^{2}_{1}g_y(x))$ depending only on the local coordinate x along the element, can be expressed as nodal loads at both beam end nodes using the incremental virtual work principle:

$$ {}^{2}_{1}\mathbf{p} = \int_0^{{}^{1}L} \mathbf{N}^{\mathrm{T}}\,{}^{2}_{1}\mathbf{g}\,{}^{1}\mathrm{d}x. \tag{62} $$

If the nodal loads depend on the displacements $\mathbf{u}$ produced by its own application, or on the deformed direction given by the final element end node coordinates ${}^{1}\mathbf{x}_a$ and ${}^{1}\mathbf{x}_b$, this dependency can be treated using

$$ {}^{2}_{1}\mathbf{p} = {}^{2}_{1}\mathbf{p}(\mathbf{u}, {}^{2}\mathbf{x}_i) \quad \text{with } i = a, b. \tag{63} $$

The Taylor expansion of these load expressions gives

$$ {}^{2}_{1}\mathbf{p}(\mathbf{u}, {}^{2}\mathbf{x}_i) = {}^{2}_{1}\mathbf{p}(\mathbf{0}, {}^{1}\mathbf{x}_i) + \left[\left.\frac{\partial\,{}^{2}_{1}\mathbf{p}(\mathbf{u}, {}^{1}\mathbf{x}_i)}{\partial\mathbf{u}}\right|_{\mathbf{u}=\mathbf{0}}\right]\mathbf{u} + \left[\left.\frac{\partial\,{}^{2}_{1}\mathbf{p}(\mathbf{u}, {}^{1}\mathbf{x}_i)}{\partial\mathbf{x}_i}\frac{\partial\mathbf{x}_i}{\partial\mathbf{u}}\right|_{\mathbf{u}=\mathbf{0}}\right]\mathbf{u} \quad (i = 1, 2). \tag{64} $$

Applying the same procedure that was used with the constant actions, the displacement dependent forces can be treated as

$$ {}^{2}_{1}\overline{\mathbf{p}} = \int_{{}^{1}L} \overline{\mathbf{N}}^{\mathrm{T}}\,{}^{2}_{1}\mathbf{p}\big|_0\,{}^{1}\mathrm{d}s + \left[\int_{{}^{1}L} \overline{\mathbf{N}}^{\mathrm{T}}\left.\frac{\partial\,{}^{2}_{1}\mathbf{p}}{\partial\mathbf{u}}\right|_0\overline{\mathbf{N}}\,{}^{1}\mathrm{d}s\right]\overline{\mathbf{u}} + \left[\int_{{}^{1}L} \overline{\mathbf{N}}^{\mathrm{T}}\left.\frac{\partial\,{}^{2}_{1}\mathbf{p}}{\partial\mathbf{x}_i}\frac{\partial\mathbf{x}_i}{\partial\mathbf{u}}\right|_0\overline{\mathbf{N}}\,{}^{1}\mathrm{d}s\right]\overline{\mathbf{u}} \tag{65} $$

and also

$$ {}^{2}_{1}\overline{\mathbf{p}} = {}^{2}_{1}\overline{\mathbf{p}}_0 + \mathbf{k_{L1}}\overline{\mathbf{u}} + \mathbf{k_{L2}}\overline{\mathbf{u}} \tag{66} $$

where

$$ {}^{2}_{1}\overline{\mathbf{p}}_0 = {}^{2}_{1}\overline{\mathbf{p}} = \int_{{}^{1}L} \overline{\mathbf{N}}^{\mathrm{T}}\, {}^{2}_{1}\mathbf{p}\big|_0\, {}^{1}\mathrm{d}s \tag{67} $$

$$ \mathbf{k_{L1}} = \int_{{}^{1}L} \overline{\mathbf{N}}^{\mathrm{T}} \frac{\partial\, {}^{2}_{1}\mathbf{p}}{\partial \mathbf{u}}\bigg|_0 \overline{\mathbf{N}}\, {}^{1}\mathrm{d}s \tag{68} $$

$$ \mathbf{k_{L2}} = \int_{{}^{1}L} \overline{\mathbf{N}}^{\mathrm{T}} \frac{\partial\, {}^{2}_{1}\mathbf{p}}{\partial \mathbf{x_i}} \frac{\partial \mathbf{x_i}}{\partial \mathbf{u}}\bigg|_0 \overline{\mathbf{N}}\, {}^{1}\mathrm{d}s. \tag{69} $$

Vector ${}^{2}_{1}\overline{\mathbf{p}}$ is the equivalent load vector and $\mathbf{k_{L1}}$ and $\mathbf{k_{L2}}$ are the load stiffness matrices. These matrices have been obtained for all the follower loads considered in the model. These matrices should be added to the ${}^{1}\mathbf{k}$ and ${}^{1}\mathbf{k_g}$ of the element.

3.3.3. Mass matrices

The forces due to the sea wave action are $f = f_\tau \boldsymbol{\tau} + f_\nu \boldsymbol{\nu}$, with $\boldsymbol{\tau}$ and $\boldsymbol{\nu}$ unit vectors in the normal and tangential directions of the pipeline element, respectively. The components of these forces, according to Morison et al. [27], are

$$ f_\tau = C_t \rho_w \frac{D}{2} |u_f| u_{f_\tau} \tag{70} $$

$$ f_\nu = C_M A_I \dot{u}_{f_\nu} + C_D A_D \left(u^2_{f_\nu}\right)^{\frac{1}{2}} u_{f_\nu} - C_I \rho_w \frac{\pi D^2}{4} \left(\ddot{u}_\nu + \dot{u}_{f_\nu}\right) \tag{71} $$

with $f_\nu = f^0_\nu + f^1_\nu$, and

$$ f^0_\nu = C_M A_I \dot{u}_{f_\nu} + C_D A_D \left(u^2_{f_\nu}\right)^{\frac{1}{2}} u_{f_\nu} - C_I \rho_w \frac{\pi D^2}{4} \dot{u}_{f_\nu} \tag{72} $$

$$ f^1_\nu = -C_I \rho_w \frac{\pi D^2}{4} \ddot{u}_\nu. \tag{73} $$

It can be observed that if f_τ and f^0_ν are static follower loads, then these loads can be treated as indicated before. However, f^1_ν generates an inertial term due to the fluid that follows the movement of the pipe. This additional load can be expressed by the following equation in which the nonlinear terms of the displacements have been eliminated:

$$ {}^{2}_{1}\mathbf{p_0} = -C_I \rho_w \frac{\pi D^2}{4} \left[\int_{{}^{1}L} \overline{\mathbf{N}}^{\mathrm{T}}\, {}^{1}\boldsymbol{\nu}\, {}^{1}\mathrm{d}s\right] \ddot{\overline{\mathbf{u}}}_\nu = {}^{2}_{1}\mathbf{m_0}\ddot{\mathbf{u}} \tag{74} $$

where ${}^{2}_{1}\mathbf{m}_0$ is the added fluid mass matrix.

Finally, in addition to the above inertial forces there exist inertial forces due to the movement of the self-weight of the pipeline, both before and after flooding. In the general case of a partially flooded element with a relative length of water given by λ, where $\lambda \in (0, 1)$, the lumped mass matrix is

$$ \mathbf{m} = \mathrm{diag}\,[m_a, m_a, 0, m_b, m_b, 0] \tag{75} $$

in which no rotational inertial forces are considered, and

$$ m_a = \frac{\lambda(2-\lambda)}{2} q_1\, {}^{1}L + \frac{(1-\lambda)^2}{2} q_0\, {}^{1}L; $$

$$ m_b = \frac{\lambda^2}{2} q_1\, {}^{1}L + \frac{1-\lambda^2}{2} q_0\, {}^{1}L \tag{76} $$

where q_0 is the empty pipe mass per unit length and q_1 is the flooded pipe mass per unit length.

3.3.4. Damping matrix

The numerical solution of the dynamic nonlinear equations of the pipeline requires the explicit derivation of a damping matrix. This can be done using experimental data where a different damping coefficient is obtained for each natural frequency. The simplest way of finding the damping matrix $\mathbf{C}$ for the whole structure is to assume an orthogonal damping matrix and to use the Rayleigh damping matrix, given by the expression

$$ \mathbf{C} = \alpha\mathbf{M} + \beta\mathbf{K} \tag{77} $$

with $\mathbf{M}$ and $\mathbf{K}$ being the linear matrices of mass and stiffness of the whole structure and α and β representing the coefficients to be found experimentally.

3.4. Dynamic equations of the pipeline

The final structure of the assembled matrix of dimension $3N$ with N the number of pipeline nodes is

$$ \left({}^{1}\mathbf{K_L} + {}^{1}\mathbf{K_{NL}}\right)\overline{\mathbf{U}} + {}^{1}\mathbf{M}\ddot{\overline{\mathbf{U}}} = {}^{2}_{1}\mathbf{R}_0 - {}^{2}_{1}\mathbf{P}_0 + {}^{2}_{1}\mathbf{P_n} - \left({}^{1}\mathbf{K_{L1}} + {}^{1}\mathbf{K_{L2}}\right)\overline{\mathbf{U}} - {}^{2}_{1}\mathbf{M}\ddot{\overline{\mathbf{U}}} \tag{78} $$

with $\overline{\mathbf{U}}$ $(3N \times 1)$ being the vector that contains the displacements and rotations of all the degrees of freedom, and ${}^{1}\mathbf{K_L}y\ {}^{1}\mathbf{K_{NL}}$ being the linear and nonlinear load matrices due to all the pipeline elements; ${}^{1}\mathbf{M}$ is the added mass matrix and ${}^{2}_{1}\mathbf{M}$ the water added mass matrix of each element. The consistent added load matrices are expressed by the term ${}^{2}_{1}\mathbf{P}_0 + {}^{2}_{1}\mathbf{P_n}$, and directly applied nodal loads are given by ${}^{2}_{1}\mathbf{R}_0$.

If the damping matrix $\mathbf{C}$ is introduced and a reordering is carried out, the following equation is reached:

$$ \mathbf{M}\ddot{\overline{\mathbf{U}}} + \mathbf{C}\dot{\overline{\mathbf{U}}} + \mathbf{K}\overline{\mathbf{U}} = \mathbf{R}(t) \tag{79} $$

with

$$ \mathbf{K} = {}^{1}\mathbf{K_L} + {}^{1}\mathbf{K_{NL}} + {}^{1}\mathbf{K_{L1}} + {}^{1}\mathbf{K_{L2}} \tag{79.a} $$

$$ \mathbf{M}(t) = \mathbf{M} = {}^{1}\mathbf{M} + {}^{2}_{1}\mathbf{M} \tag{79.b} $$

$$ {}^{1}\mathbf{R}(t) = {}^{2}_{1}\mathbf{P}_0 - {}^{2}_{1}\mathbf{P}_0 - {}^{2}_{1}\mathbf{P_n}. \tag{79.c} $$

4. Computer program

In order to implement the structural model described here, a computer program has been written. This program has been developed within the framework of ANSYS, a commercial finite element computer program. In this way, the ANSYS capabilities for nonlinear analysis and postprocessing are available. However, ANSYS is unable to handle the sequential analysis produced by the different structures. These are caused by the barge movement and the continuous filling of the pipeline in the framework of a geometric nonlinear analysis, i.e. new element introduction, changes in boundary conditions, and pipeline geometry.

The computer program developed is composed of 46 subroutines and has been written in the ANSYS programming language APDL. This language is similar to FORTRAN and some of its capabilities are: (1) to include matrices that are used by the computer program, (2) to take decisions within ANSYS execution time according to the obtained results, and (3) to write data and results files with arbitrary format.

The nonlinear analysis of the pipeline laying on the seabed is carried out using an incremental–iterative procedure as described in [29]. The main computational steps included in the APDL program are summarized as follows:

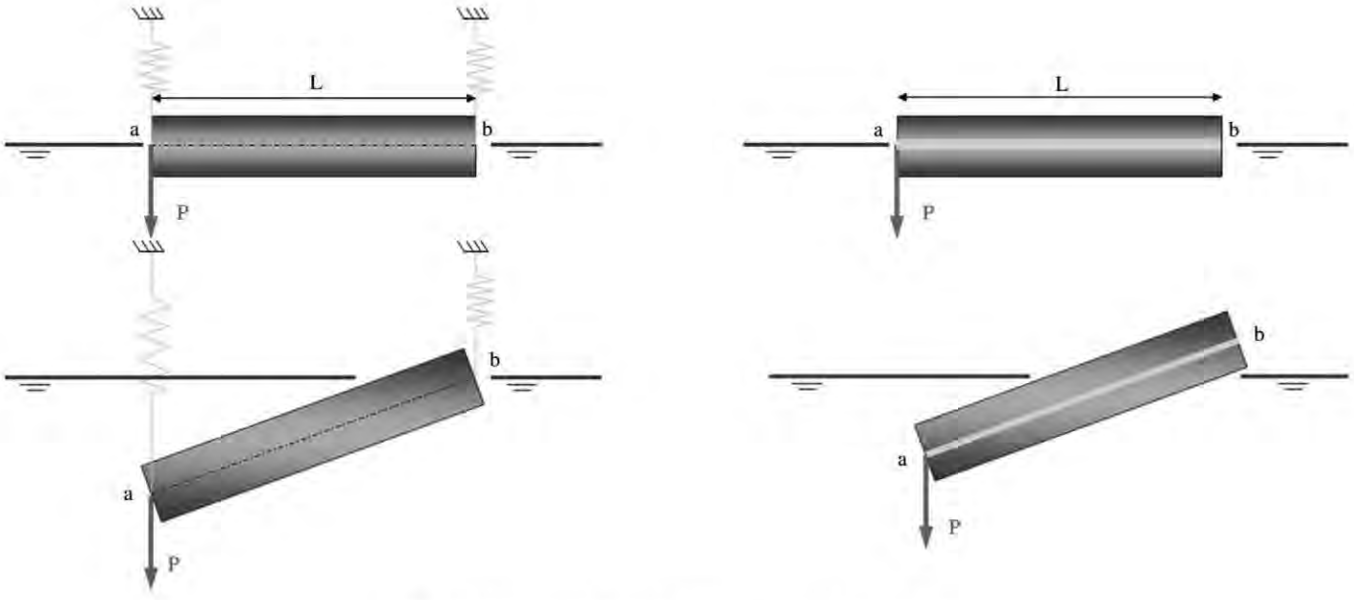

Fig. 6. Follower forces due to Archimedes force validation models.

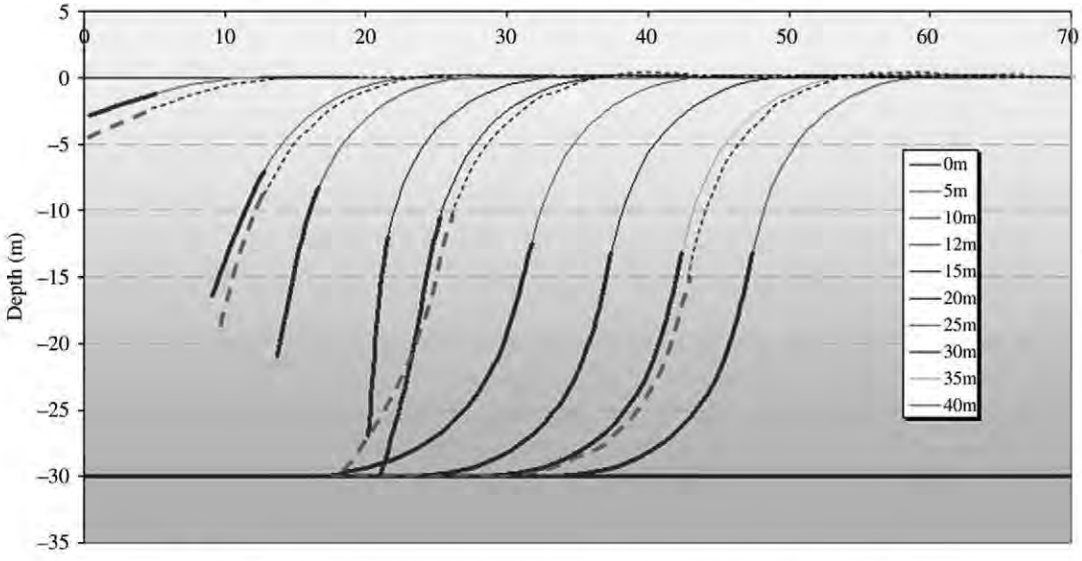

Fig. 7. Displacement comparison between the model in [1] and the present model [2].

Table 1
Displacements at the top (node 1), and reactions at the bottom.

Model	u_1 (m)	v_1 (m)	θ_1 (rad)	R_x (kN)	R_y (kN)	M_z (m kN)
1	0.5462399	0.00	0.0728317	−1.9995	0.00	9.996
2	0.5465449	-1.0775×10^{-4}	0.072877	−1.9999	0.10931	10.000

1. Define the initial pipeline configuration C_0 (loads and boundary conditions).
2. Compute within a UL formulation the target equilibrium C_2 from the current configuration C_1:
   (a) Update the pipeline geometry and the existing stresses with the last equilibrium configuration C_1.
   (b) Apply the new load step (hydrostatic pressure, water fill, horizontal load) or change the barge position. The objective of the following computational steps is to obtain the equilibrium target configuration C_2.
   (c) Compute and input the load stiffness matrices due to all the follower loads. This is carried out creating new elements with the same two nodes of each finite beam element.
   (d) Solve the incremental nonlinear equilibrium equations between C_1 and C_2. This step is carried out completely by ANSYS. Geometrical nonlinear effects and nonlinear boundary conditions are considered.
   (e) Obtain the loads corresponding to the deformed shape configuration C_2.
   (f) Compare the difference D between the applied and obtained load at each node with a given tolerance δ.
      i. If $D < \delta$ load convergence exists. The small displacement hypothesis should be checked as follows.
         A. If $\|\mathbf{u}\| < \varepsilon$ i.e. small displacement hypothesis is valid, then go to point 3.

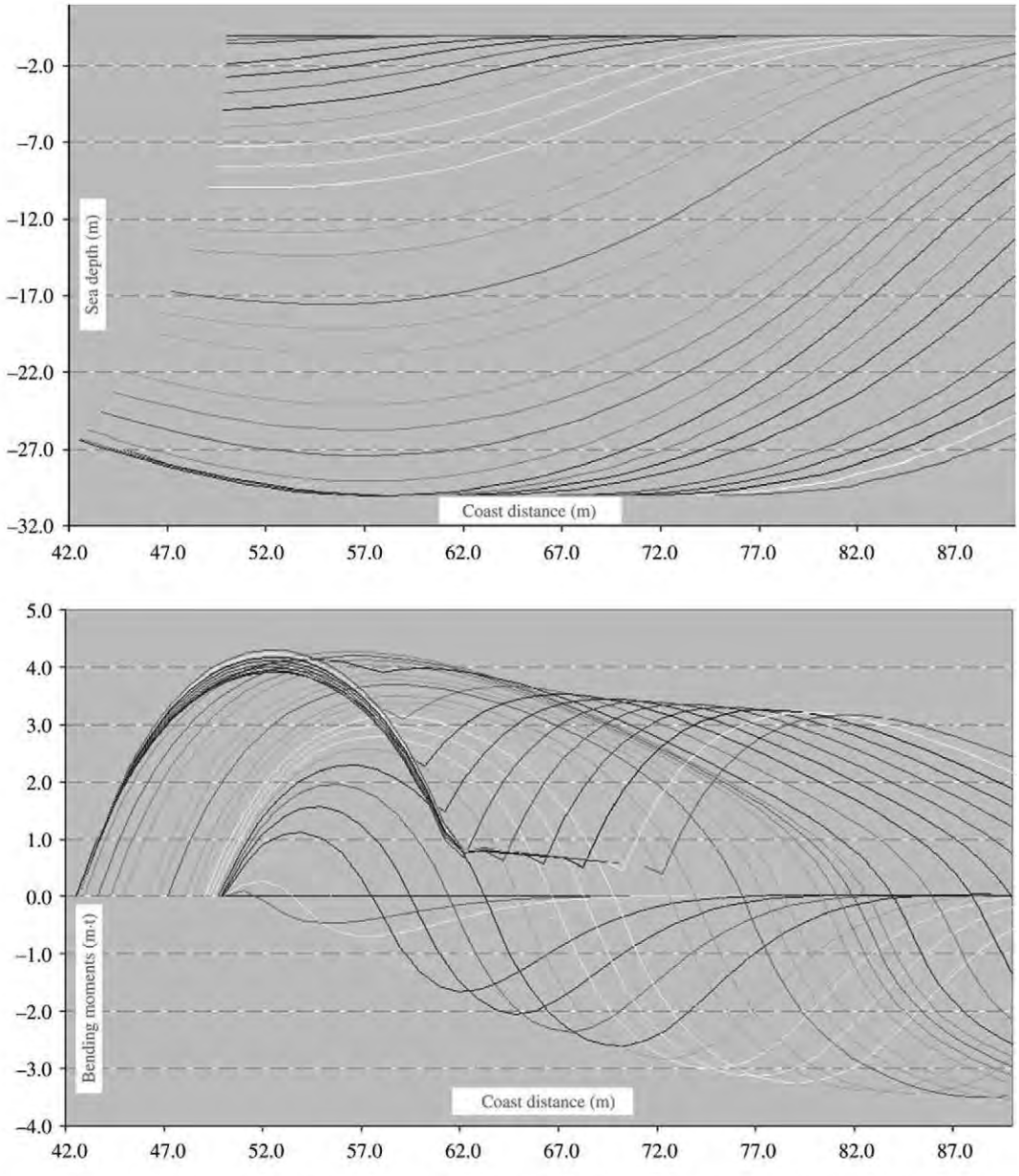

Fig. 8. Displacements and bending moments with an axial load of 5 t (1 t = 10 kN) and cable at the coast.

B. if $\|\mathbf{u}\| > \varepsilon$ i.e. small displacement hypothesis is not valid, then the current load step must be subdivided and each load substep should be considered as a new step. The execution will continue at point 2.

Here $\|\mathbf{u}\|$ is the incremental displacement vector norm and ε a small given tolerance.

ii. If $D < \delta$ load convergence does not exist, then return to point 2a and use the obtained loads found in point 2e in order to be applied in point 2b.

3. Output the results of this load step.
4. Generate a new geometry from the deformed equilibrated one (configuration C_2) of the previous iteration, i.e. change C_2 to C_1.
5. Input the computed stresses in this geometry as initial stresses in configuration C_1 at each beam finite element node.
6. Repeat from point 2 until all the load steps are completed.

In order to validate the proposed computational model, several examples have been developed, as shown in the next section.

4.1. Validation examples

The validity of the computer program has been checked by comparing the results obtained with those published in the literature and also with theoretical results of simple cases. In the following only three examples are given. The following standard data have been used:

$R_{ext} = 0.40$	Outer pipe radius	m
$R_{int} = 0.375$	Inner pipe radius	m
$p_{pipe} = 2.6833$	Self-weight of the pipeline, as measured in air	kN/m
$E_{pipe} = 2.0 \times 10^5$	Young modules of the pipeline	kN/m^2
$\gamma = 10.0$	Specific weight of water	kN/m^3

In the first example, the accuracy of the flotation model for the buoyancy forces is shown. A rigid beam element *ab* of length L is floating at level $y = 0$, i.e. its self-weight is equilibrated by the hydrostatic pressure, as shown in Fig. 6. In addition, the beam is subjected to a small vertical force P at node a. The horizontal

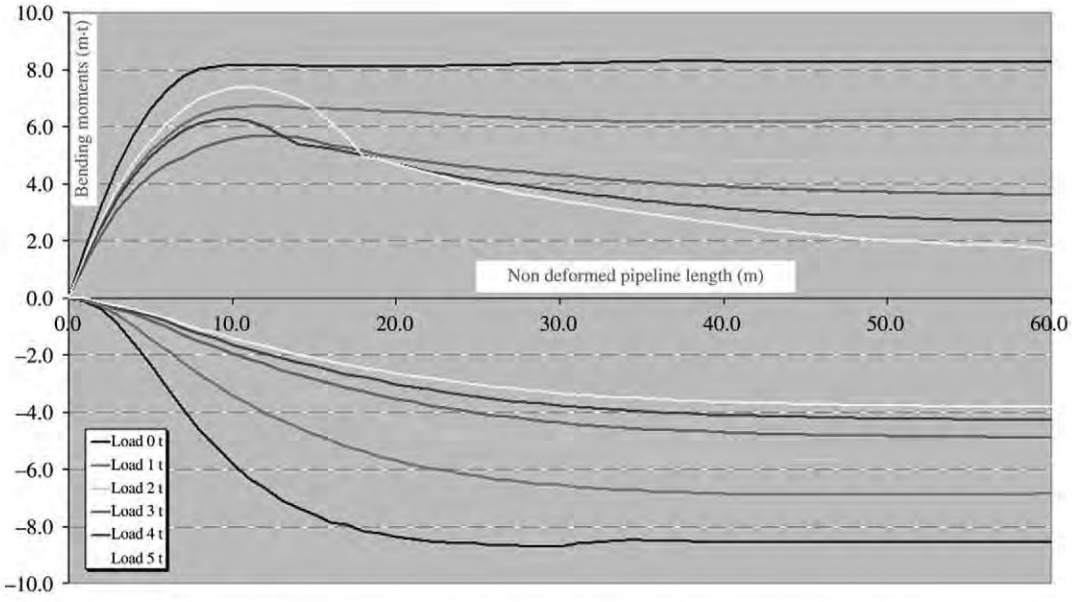

Fig. 9. Bending moments envelopes for axial load varying from 0.0 to 5.0 t (1 t = 10 kN).

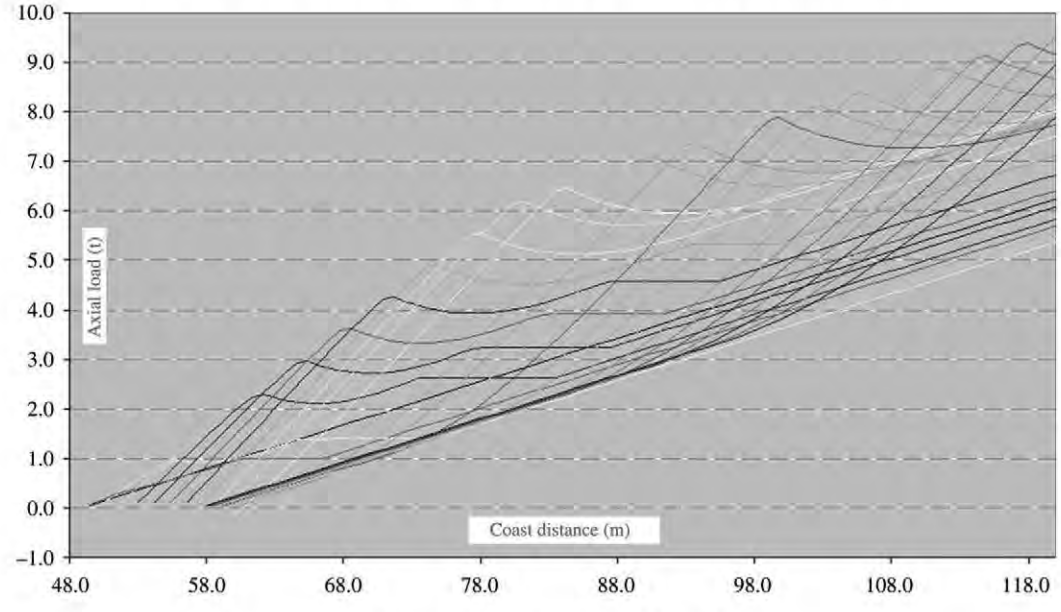

Fig. 10. Axial load for $C_t = 0.07$ and $C_D = 0.7$.

displacement at node a is restrained. In a first analysis buoyancy is simulated by introducing nonlinear springs at two element nodes. In the second analysis a follower load stiffness matrix is used. The node vertical displacement results of the first analysis (Fig. 6, left) are $u_a = \frac{P}{k}$ and $u(b) = 0$, with $k = k_t(0)$ the tangent nonlinear spring stiffness. However, the results of the second analysis (Fig. 6, right) are $u_a = \frac{6P}{kL}$ and $u_a = -\frac{3P}{kL}$, in agreement with the theoretical ones.

In order to validate the follower forces due to the horizontal constant current, a second example has been carried out. A vertical cantilever beam element, fixed at the bottom, has been modeled with ten finite elements. The total length of the beam is $L = 10$ m. The Young's modulus of the pipeline material for this example has been reduced to the value $E_{pipe} = 100\,000$ kN/m^2 in order to increase the displacements.

The model verifies the horizontal displacements at the top node and the reactions at the bottom. Two analyses have been carried out. In the first one (model 1) a simple beam is considered and in the second one (model 2) the follower load stiffness matrix has been added. The difference between these two analyses is that in the first one the loads keep the same horizontal direction and magnitude, whereas in the second one the loads are follower force forces, i.e. they remain normal to the deformed axis of the beam. An uniform load of intensity $q = 0.2$ kN/m has been applied. The ANSYS results of displacements and reactions for both cases are shown in Table 1.

In model 1, the horizontal reaction is $R_y = 0$, which is consistent with the load horizontal direction hypothesis. In model 2, the computed value given in Table 1 for the horizontal reaction is $R_y = 1.0931$. This value can be verified by numerically solving the integral $\int_0^L q(x) \sin\theta dx = 0.01092$, with $\theta(x)$ the slope angle of the beam elastic at section x.

Finally, a more elaborate example than the two previous ones is shown. The structural behavior of a simple laying process of a floating pipeline by continuous inundation is simulated by two models, a rather simplified model and the proposed one.

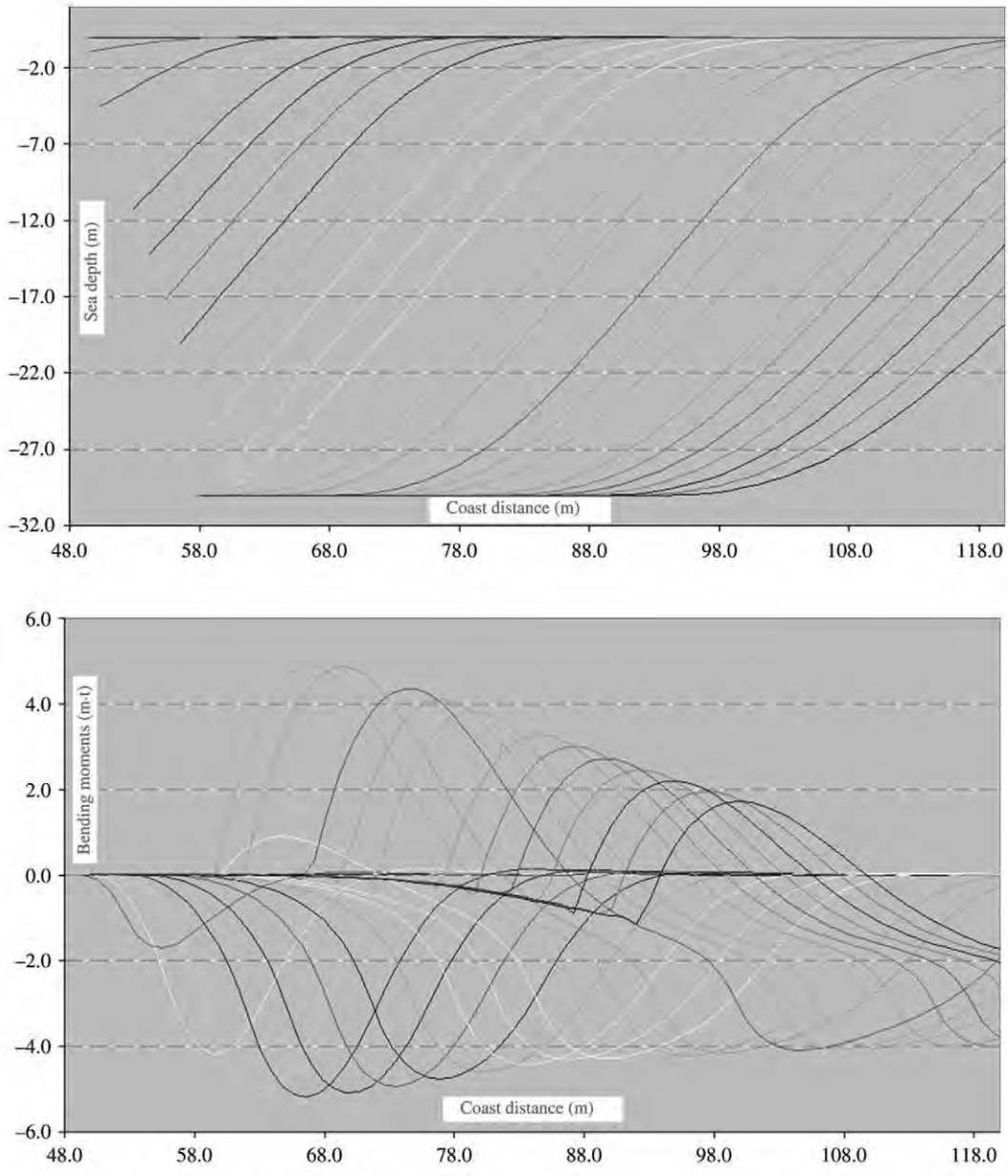

Fig. 11. Displacements and bending moments for $C_D = 0.70 y C_t = 0.07$.

A comparison between them is carried out. The first model has been developed in [1] and it introduces several simplifications, among them: (1) buoyancy is simulated by equivalent linear springs and pipeline self-weight reduction, (2) beam elements are modeled by isoparametric finite elements of the type C_0, (3) the seabed is horizontal, (4) the barge position is static, and (5) external axial load, current, and wave actions are not considered. The barge remains at a fixed position at a distance of 121 m from the original pipeline end. The results obtained by these two models are shown in Fig. 7, in which discontinuous lines correspond to results from [1] and continuous lines are results of the present model. It can be observed that the displacement and bending moment resulting from both models agree reasonably well. More details about this comparison can be found in [2,29].

4.2. Applied numerical examples

Fig. 8 shows the deformed shapes and the bending moments of the pipeline during the laying process. The pipeline is located 50 m from the coast and placed at a depth of 30 m when an axial control load of 50 kN is applied from the barge. The coast end is joined to the pipeline by means of a steel cable.

Fig. 9 represents six bending moment envelopes of the same pipeline laying process for the axial load at the barge varying between 0 and 50 kN.

Fig. 10 shows the axial load variation along the same pipeline during its laying process subjected in addition to current actions. The current is applied from sea water depth to the coast without any axial load due to the barge. The normal drag and tangential drag coefficients used in this case have been the following ones: $C_D = 0.70$ and $C_t = 0.07$, respectively. The axial force variation shown is due to the friction of the current along the outfall. Finally, in Fig. 11, the same displacements and bending moments as in Fig. 10 are shown.

From these examples it can be observed that the pipe deformation and forces change with the control parameters described earlier, such as the axial load, and also with the influence of currents. Any of these input parameters can be varied, leading to a clear and straightforward optimization process.

5. Conclusions

This paper presents a model of the structural behavior of a floating pipeline during the laying process. The expressions for the stiffness matrices of the follower loads due to hydrostatic pressure, current, and sea waves have been developed. Also, the transformation of the velocity and acceleration fields into forces acting on the outfall pipeline has been fully investigated. These fields have been numerically evaluated at each point in space and time according to the Airy Wave Linear Theory.

A convergence process at each load step has been developed with a displacement control error mechanism in order to accurately deal with the small deformation formulation used between consecutive computational steps.

The model emphasizes the importance o applied follower forces representing the hydrostatic pressure pipeline region close to the free surface of the water. In f. when the results obtained are compared with those from other simplified models, which use springs or a reduction in self-weight, it is noted that the influence of hydrostatic pressure can be very important.

The model has been implemented and tested in a computer program. The pipeline construction has been simulated using small steps to represent the continuous process. Some examples have been developed to show the capabilities of the software, as well as the significance of some of the parameters acting on the process.

Finally, this model can be used to optimize the laying process. Objective functions that describe stresses or curvatures along the pipeline can be minimized by choosing the best combination of control variables. These variables can be modified dynamically in time, during the laying process. For example, at each computational step (or in real time in an actual pipeline laying process) various parameters can be modified, such as the inundated length of the pipeline, the axial load applied at the barge, or the position of the barge itself.

References

[1] Oliver J. Una formulación intrínseca para el estudio, por el método de los elementos finitos, de vigas, arcos, placas y láminas, sometidos a grandes corrimientos en regimén elastoplástico. Ph.D. thesis. Escuela Técnica Superior de Ingenieros de Caminos, Canales y Puertos. Universidad Politécnica de Cataluña. 1982.

[2] García-Palacios J, Samartín A, Negro V. Modelo del cálculo del proceso de fondeo de un emisario submarino. In: Proceedings de Métodos Computacionais em Engenharia. 2004.

[3] Kirk DE. Optimal control theory: An introduction. Englewood Cliffs (NJ): Prentice-Hall; 1970.

[4] API. Comparison of marine drilling analyses. In: Bulletin 2J. American Petroleum Institute; 1977.

[5] Chakrabarti SK. Hydrodynamics of offshore structures. WIT Press/ Computational Mechanics Publications; 1987.

[6] Patel MH, Seyed FB. Review of flexible riser modelling and analysis techniques. Eng Struct 1995;17(4):293–304.

[7] Bratu Ch, Narzul P. Dynamic behaviour of flexible risers. Amsterdam, The Netherlands: BOSS; 1985.

[8] Orgill G, Wilson JF, Schmertmann GR. Static design of mooring arrays for offshore guyed towers. Appl Ocean Res 1985;7(3):166–74.

[9] Datta TK, Bassu AK. Stress analysis of submarine pipelines. Proceeding of the Inst Civil Eng 1977;63:833–41.

[10] Ahmad S, Datta TK. Nonlinear response analysis of marine risers. Comput Struct 1992;43(2):281–95.

[11] Lambrakos KF. Marine pipeline dynamic response to waves from directional wave spectra. Appl Ocean Res 1982;9(4):385–405.

[12] Wilson EL. SAP. A Structural Analysis Program. Report UC SESM 70-20. Berkeley: University of California, Earthquake Engineering Research Center; 1970.

[13] ABAQUS. Getting started with ABAQUS/standard. USA: Hibbit, Karlsson and Sorensen Inc.; 1998.

[14] De Salvo GJ. ANSYS engineering analysis system. Verification manual. Houston (PA): Swanson Analysis System Inc.; 1985.

[15] Schweizerhof K, Ramm E. Displacement dependent pressure loads in nonlinear finite element analysis. Comput Struct 1984;18(1):1099–114.

[16] Chung JS, Whitney AK, Loden WA. Nonlinear transient motion of deep ocean mining pipe. J Energy Res Tech ASME 1981;103:2–10.

[17] Chakrabarti SK. Inline forces on fixed vertical cylinder in waves. J Waterw Port Coastal Ocean Div 1980;106:145–55.

[18] Kalliontzis C. Numerical simulation of submarine pipelines in dynamic contact with a moving seabed. Earthq Eng Struct Dyn 1998;27:465–86.

[19] Guarracino F, Mallardo V. A refined analytical analysis of submerged pipelines in seabed laying. Appl Ocean Res 1999;21:281–93.

[20] Palmer A. Pipelaying in deep waters. J Offshore Tech 1994;2:13–7.

[21] Vikestad K, Vandiver JK, Larsen CM. Added mass and oscillation frequency for a circular cylinder subjected to vortex-induced vibrations and external disturbance. J Fluids Struct 2000;14:1071–88.

[22] Zhu DS, Cheung YK. Optimization of buoyancy of an articulated stinger on submerged pipelines laid with a barge. Ocean Eng 1997;24(4):301–11.

[23] Safai VH. Nonlinear dynamics analysis of deep water risers. Appl Ocean Res 1983;5(4):215–25.

[24] Construction Industry Research and Information Association. Manual on the use or rock in coastal and shoreline engineering. Report 154. Centre of Civil Engineering Research and Codes. 1983. Reprinted 1991.

[25] García-Palacios J, Samartín A. An analysis of installation of submarine pipelines. In: Proc. of the IASS conference of Madrid. shells and spatial structures: From recent past to the next millennium. 1999. p. C1.101, C1.116.

[26] Pellón-Arrieta L. Emisarios submarinos. Technical report. Saneamientos Marítimos S.A. Mandri 25, 08022 Barcelona, España; 1982.

[27] Morison JR, O'Brien MP, Johnson JW, Schaaf S. The force exerted and surface waves on piles. Petrol Trans, AIME 1950;189:149–54.

[28] Yang YB, Kuo SR. Theory and analysis of nonlinear frame structures. Prentice Hall; 1994.

[29] García-Palacios J. Análisis tensional del proceso constructivo de emisarios flotados y fondeados. Ph.D. thesis. Madrid, Spain: Escuela Técnica Superior de Ingenieros de Caminos, Canales y Puertos. Technical University of Madrid; 2004, http://oa.upm.es/311/01/04200426.pdf.